Journal of Power Sources 264 (2014) 248–253

Contents lists available at ScienceDirect

Journal of Power Sources

journal homepage: www.elsevier.com/locate/jpowsour

Carnation-like MnO_2 modified activated carbon air cathode improve power generation in microbial fuel cells

Peng Zhang [a], Kexun Li [a,*], Xianhua Liu [b,**]

[a] School of Environmental Science and Engineering, Nankai University, Tianjin 300072, PR China
[b] School of Environmental Science and Engineering, Tianjin University, Tianjin 300072, PR China

HIGHLIGHTS

- γ-MnO_2 decorated AC air cathode was produced by using a simple potentiostatic method.
- Carnation-like MnO_2 crystals were formed on the cathode surface.
- The mesopore structure plays an important role in the cathode performance.
- The highest maximum power density of 1554 mW m^{-2} was achieved.
- The simple cathode preparation method may promote the application of MFC technology.

ARTICLE INFO

Article history:
Received 15 January 2014
Received in revised form
16 April 2014
Accepted 17 April 2014
Available online 30 April 2014

Keywords:
Microbial fuel cell
Manganese oxide
Electrodeposition
Oxygen reduction reaction

ABSTRACT

Highly active and low-cost electrocatalysts are of great importance for large-scale commercial applications of microbial fuel cells (MFCs). In this work, we prepared an activated carbon (AC) air cathode containing electrodeposited γ-MnO_2 using a potentiostatic method. The results indicated that carnation-like MnO_2 crystals were bound to the surface of the AC air cathode after a deposition time of 10 min, which greatly improved the performance of the cathode. BET analysis results demonstrated that the electrodeposition of MnO_2 decreased the micropore surface area of the cathode but increased the mesopore surface area. When compared with a bare AC air cathode, the electrodeposited MnO_2 cathode exhibited higher catalytic activity for oxygen reduction reaction. The maximum power density of the MFC equipped with the electrodeposited MnO_2 AC air cathode was 1554 mW m^{-2}, which is 1.5 times higher than the control cathode.

1. Introduction

The microbial fuel cell (MFC) is a biotechnology that utilises bacteria to create clean and renewable electrical energy by oxidising organic substances in wastewater and represents a promising alternative for generating power [1,2]. The single-chambered design containing an air cathode has attracted considerable attention due to its low cost and simple construction [3,4]. However, the cell s' low power production still limits its practical application.

Previous research has determined that the oxygen reduction reaction (ORR) on the cathode is a limiting step for electricity production [5]. The ORR rate is a major factor to be considered in the design of low-cost and high-efficiency MFCs. Platinum (Pt) is a highly active catalyst and has been used to improve the ORR rate [6,7]. However, because of Pt's high cost and low catalytic stability due to poisoning [8,9], low-cost non-Pt catalysts should be developed. Activated carbon (AC) has received much attention due to its excellent performance in oxygen reduction reactions on the cathode. Zhang et al. found that AC air cathode exhibited an equivalent performance to Pt carbon cloth cathode after AC was fixed on nickel mesh with polytetrafluoroethylene (PTFE) as the binder [5]. AC air cathodes made using the rolling-press method showed extremely high power output and reproducibility [10,11]. Chen et al. reported an inexpensive AC-based air cathode prepared using a simple painting method, which could reach a maximum power density of 861 mW m^{-2} [12]. AC was used as a catalyst and nickel foam was used a as current collector, resulting in an MFC that produced a power density of 1190 mW m^{-2} [13]. Pyrolysed iron ethylenediaminetetraacetic acid [4], alkaline conditions [14], and

* Corresponding author. School of Environmental Science and Engineering, Nankai University, Tianjin 300072, PR China. Tel./fax: +86 22 23495200.
** Corresponding author. School of Environmental Science and Engineering, Tianjin University, Tianjin 300072, PR China. Tel./fax: +86 22 27402367.
E-mail addresses: likx@nankai.edu.cn (K. Li), lxh@tju.edu.cn (X. Liu).

http://dx.doi.org/10.1016/j.jpowsour.2014.04.098
0378-7753/

ammonia gas [15] have also been used to enhance AC performance as an ORR catalyst in MFCs. However, more efficient and lower cost modifications should be further explored to enhance the practical applications of AC air cathodes.

Manganese dioxide has previously been studied as a highly chemical stable, eco-friendly and cost-effective alternative to Pt in fuel cells [16–18]. Zhang et al. studied the catalytic properties of three manganese dioxide structures (α, β and γ MnO_2) bound to graphite on air cathodes in MFCs [17]. Liu et al. demonstrated that a nano-structured MnO_x material on carbon paper prepared using an electrochemical deposition method could be an effective catalyst for oxygen reduction [19]. In other studies, MnO_2/carbon nanotubes [20–22], MnO_2 nanoparticles confined in ordered mesoporous carbon [23] and a MnO_2-graphene hybrid [16,24] were also fabricated as air cathodes in MFCs. Although these modifications were found to improve the performance of AC air cathodes, these processes are complicated and costly, which has limited their large-scale application.

In this paper, an AC air cathode decorated by MnO_2 was prepared using a simple steady state potentiostatic method, in which AC acted as both a supporting plate and a conductive substrate for the MnO_2 catalyst. To our knowledge, this is the first report of the direct combination of MnO_2 and an AC composite as a cathode catalyst for ORR in MFCs. The influence of deposition time on cathode performance was investigated. The prepared AC air cathodes were characterised by linear sweep voltammetry (LSV), scanning electron microscopy (SEM), Brunauer–Emmett–Teller (BET) surface area analysis, X-ray diffraction (XRD) and X-ray photoelectron spectroscopy (XPS). The performances of MFCs equipped with the prepared AC air cathodes were also examined.

2. Experimental

2.1. Electrode preparation

Cathodes were constructed using the rolling method as previously described by Dong [25]. MnO_2 was electrodeposited using a three-electrode system at room temperature as shown in Fig. 1. The AC air cathode used as working electrode was washed with distilled water and dried in an oven before testing, and placed on the open side of the plastic cylindrical chamber with the gas diffusion layer facing the air and AC catalyst layer facing the electrolyte. A Pt wire was used as the counter electrode and a saturated calomel electrode (SCE) was used as the reference electrode. The electrolyte was composed of 0.1 M Na_2SO_4 and 0.1 M $Mn(CH_3COO)_2$, which was similar to electrolytes used in previous studies [26]. The MnO_2 AC air cathodes were prepared using a potentiostatic method under 0.6 V (vs. SCE) for 5, 10 and 15 min with agitation. After electrodeposition, the prepared electrode was washed with distilled water and dried in an oven at 80 °C for 12 h.

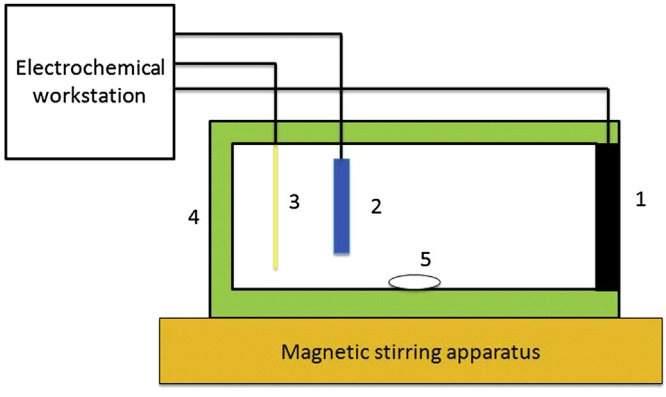

Fig. 1. Schematic of the electrochemical deposition system. 1, AC air cathode (working electrode); 2, saturated calomel electrode (reference electrode); 3, Pt wire electrode (counter electrode); 4, plastic cylindrical chamber; 5, rotor.

2.2. MFC setup and operation

The MFCs were constructed with a cylindrical plastic chamber (28 mL). The space between electrodes was 4 cm. Both the anode and cathode had the same projected area of 7 cm^2. The anode was composed of carbon felt, which was cut into a round shape with a thickness of 0.5 cm and a diameter of 3 cm. The cathodes were placed in the chamber as previously described [3]. Titanium wires were used to connect the anode and cathode to the external resistance. The cathodes were constructed in the same MFC equipment to ensure the same experimental conditions. Reactors were fed with 50 mM phosphate buffer solution (PBS: Na_2HPO_4, 4.09 g L^{-1}; $NaH_2PO_4{\cdot}2H_2O$, 3.32 g L^{-1}; KCl, 0.13 g L^{-1}; NH_4Cl, 0.31 g L^{-1}), 12.5 mL L^{-1} trace minerals and 5 mL L^{-1} vitamins [27]. 1 g L^{-1} sodium acetate served as the carbon source [28]. The external resistance was fixed at 1000 Ω. All experiments were conducted in a 30 °C incubator.

2.3. Analysis and calculations

The voltages were monitored using an 8-channel voltage collection instrument (MPS-10, Morpheus Electronic Co. Ltd, Beijing, China) while the MFCs were connected to an external resistance of 1 K. To obtain a polarisation curve, the external resistance was varied from 50 to 9000 Ω. The voltage was recorded when it approached a stable state [29]. The power density was calculated according to $P = UI/A$, where U is the voltage, I is the current and A is the surface area of the cathode. The current density was calculated using $I = U/R_{ex}$, where the R_{ex} is the external resistance. The potentials of the anodes and cathodes in the tested MFCs were recorded using a voltmeter (VICTOR, VC890C+), with the anode or cathode electrode as the working electrode, and an Ag/AgCl electrode as the reference electrode.

LSV was measured to evaluate the ORR performance of each cathode at a scan rate of 0.1 mV s^{-1} from an open circuit potential to −0.3 V using an Ag/AgCl electrode (0.195 V versus standard hydrogen electrode) as the reference electrode. The LSV tests were conducted using a potentiostat (CS120, Wuhan Corrtest Instrument Co. Ltd) in a three-electrode electrochemical cell setup, which was built as a 3 cm-cubic-single-chamber reactor. A Pt electrode (projected surface area of 1 cm^2) was used as the counter electrode and the tested cathodes (projected surface area of 7 cm^2) were used as the working electrodes. Because the working potential of air cathodes in the MFC was typically in the region from 0.05 to −0.2 V, the currents that responded in this cathode potential region in LSV were typically used to evaluate the cathode performance. All experiments were conducted in a 30 °C temperature-controlled room in 50 mM PBS.

To characterise the crystal structure of the catalysts, X-ray diffraction (XRD) was carried out with a D/max-2500 X-ray generator. The X-ray intensity was measured over a diffraction 2-theta angle from 5 to 80 with a velocity of 0.02 $step^{-1}$ and 2 min^{-1}. XPS (Axis Ultra DLD, Kratos Analytical Ltd.) was also used to determine the Mn state. The binding energy values were referenced to the carbon C1s core peak at 284.7 eV. The morphology and size of the catalyst samples were examined by SEM (S-3500N, Hitachi) with an acceleration voltage of 20 kV. Specific surface area determination of the AC catalyst layer was performed using the BET

method with an adsorption meter (ASAP2020/Tristar 3000, MICROMERITICS).

3. Results and discussion

3.1. Morphological characterisation and surface area analysis

Different electrodeposition times produced MnO_2 structures with different morphologies, as shown in Fig. 2. Fig. 2a displays the AC air cathode without MnO_2, in which disordered AC particles can be observed. With a deposition time of 5 min, a small quantity of MnO_2 was found on the surface of the AC particles, as shown in Fig. 2b. The diameters of these MnO_2 crystals were less than 1 μm. When the deposition time reached 10 min, carnation-like MnO_2 structures were observed on the surface of the AC particles, as seen in Fig. 2c. The crystal diameter increased as deposition time increased. Rod-like [30], wire-like [31–33] and sheet-like [34] MnO_2 crystals produced by electrodeposition have previously been observed, but this is the first reported observation of carnation-like MnO_2 structure. A deposition time of 15 min was also applied in our study, and we determined that, as in Fig. 2d, the disordered AC particles were completely covered by the MnO_2 deposition layer and the rugged AC cathode surface became a 'flatland'.

Table 1 illustrates the BET surface area data for the bare AC cathode and the electrodeposited MnO_2 AC air cathode. The results demonstrated that the BET surface area of the samples decreased with increasing deposition time, which was clearly due to the decline in the micropore area. The BET surface area and micropore area of the bare AC catalyst layer were 1747.53 and 933.31 $m^2\ g^{-1}$, while those of the deposited MnO_2 AC layer with a deposition time of 15 min were only 1460.83 and 699.03 $m^2\ g^{-1}$, respectively. The decline of the surface area was the result of damage to the micropore structure caused by MnO_2 deposition, which agreed with the SEM result in Fig. 2. In contrast, the mesopore surface area increased from 814.22 to 894.21 $m^2\ g^{-1}$ as the deposition time increased from 0 to 10 min. This phenomenon agreed with the formation of the carnation-like structures, which had a multilayer structure. The multilayer structure of the carnation-like MnO_2 crystals increased the mesopore surface area of the MnO_2. The fraction of microporosity decreased as the deposition time increased, which may enhance the power output, as previously reported [35].

Table 1
Summary of experimental data from the BET surface area analysis of the AC catalyst layer (0 min) and the MnO_2-electrodeposited AC catalyst layer with deposition times of 5, 10 and 15 min.

Surface area	0 min	5 min	10 min	15 min
BET surface area ($m^2\ g^{-1}$)	1747.53	1611.17	1598.14	1460.83
Micropore surface area ($m^2\ g^{-1}$)	933.31	786.91	703.93	699.03
Mesopore surface area ($m^2\ g^{-1}$)	814.22	824.26	894.21	761.80

3.2. X-ray photoelectron spectroscopy and X-ray diffraction studies

Fig. 3 displays the XPS spectra of the MnO_2 standard and the film electrodeposited on the AC layer. The peaks due to Mn $2p_{3/2}$ appeared at a binding energy of 642.2 eV [26], indicating that the manganese in the electrodeposited MnO_2 was present in the chemical state of Mn (IV). The Mn $2p_{1/2}$ peaks at a bonding energy of 654.4 eV further confirmed the sole existence of Mn(IV) [36] on the surface of the AC air cathode.

Fig. 4 displays the XRD patterns of the AC cathode and the AC catalyst layer electrodeposited with MnO_2 for different deposition times. The XRD results for the AC catalyst layer indicated the presence of a combination of crystalline and non-crystalline material with diffraction peaks at approximately 17°, 26°, 44°, 50° and 74°. As the deposition time increased, the diffraction peaks became weaker, indicating that the surface of the AC electrode had been gradually covered by a film of MnO_2. Despite the low intensity and weak crystalline nature, the diffraction peaks of the AC catalyst layer electrodeposited with MnO_2, with the exception of the AC catalyst layer, can be ascribed to the crystal planes of (110), (021), and (061), especially for the AC cathode with a deposition time of 15 min, which confirmed that the electrodeposited product was γ-MnO_2 [26,37]. The diffraction peaks of γ-MnO_2 can be ascribed to the crystal planes of (110), (021) and (061) at approximately 22°, 37° and 68°, respectively, which had obvious growth, indicating that the MnO_2 accumulated as the deposition time increased and that the amount of MnO_2 on the AC air cathode increased.

3.3. Electrochemical performance

The oxygen reduction characteristics of the AC air electrode containing electrodeposited MnO_2 were analysed by LSV relative to the AC air electrode without any catalyst to determine whether the

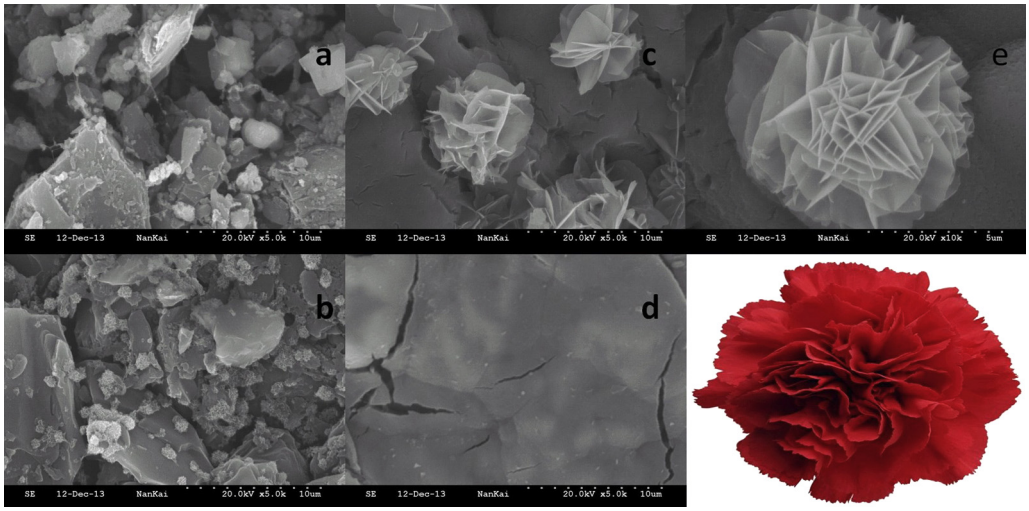

Fig. 2. SEM images of the surface of the AC air cathode (a) and the MnO_2-deposited AC air cathode with deposition times of 5 (b), 10 (c) and 15 min (d) at a magnification of 5000×. A single carnation-like crystal (e) at a magnification of 1,0000×. A photograph of a carnation flower is displayed in the picture in the lower right corner.

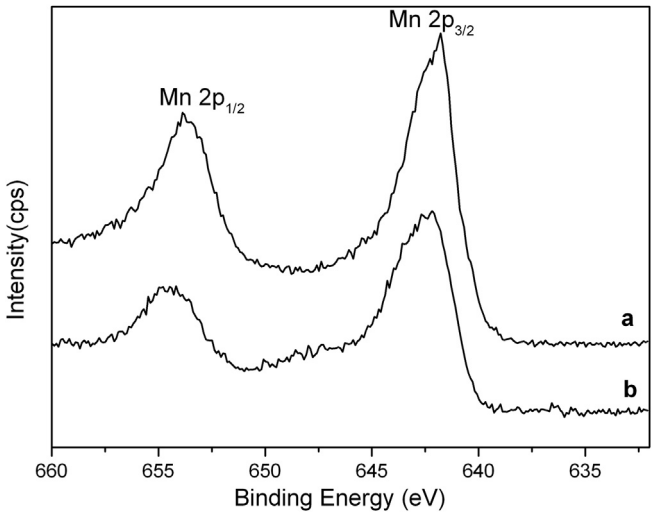

Fig. 3. XPS spectra of MnO_2 electrodeposited on the AC air cathode (a) and the MnO_2 powder standard (b).

MnO_2 catalyst contributed to the oxygen reduction reaction. Fig. 5 displays the LSV results for the AC air cathode with different electrodeposition times. At a potential of −0.1 V, the current density of the ORR at the AC air cathode with a MnO_2 deposition time of 10 min was 0.81 mA cm^{-2}, which was 2.07 times higher than that of the bare AC air electrode (0.39 mA cm^{-2}). All three AC air cathodes with deposited MnO_2 exhibited higher current densities than the bare AC air cathode, indicating that electrodeposited MnO_2 promoted the ORR on the cathode. The E_{onset} of these four electrodes increased as the amount of MnO_2 deposited on the electrode increased. The bare AC air cathode only had an E_{onset} of 0.17 V, while the E_{onset} values for the MnO_2-deposited AC air cathodes with deposition times of 5, 10 and 15 min were 0.29, 0.25 and 0.31 V, respectively, indicating that the catalytic activity increased as the MnO_2 accumulated. This tendency agreed with the results of a previous study [20], which indicated that the electrochemical activity increased as the amount of MnO_2 doped into a carbon nanotube increased.

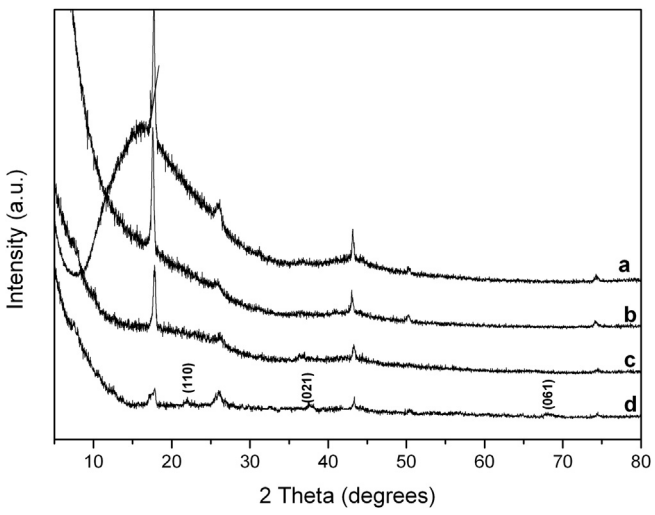

Fig. 4. XRD patterns of the AC air cathode (a) and the electrodeposited AC air cathode with deposition times of 5 (b), 10 (c) and 15 min (d).

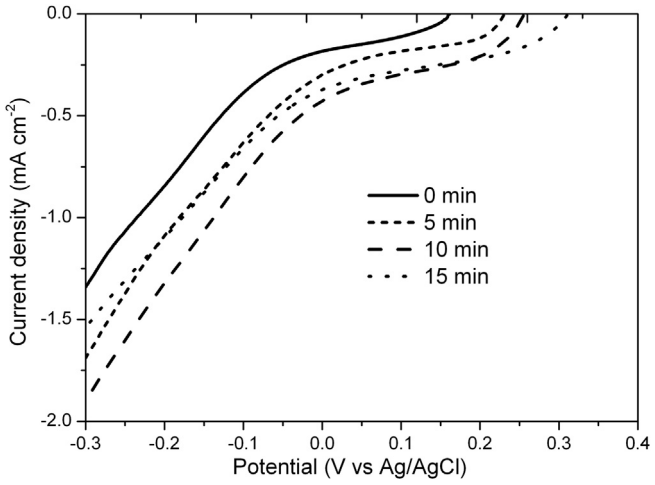

Fig. 5. LSVs of the AC air cathode and the MnO_2-electrodeposited AC air cathode with deposition times of 5, 10 and 15 min.

3.4. MFC performance

To verify the effects of the MnO_2-electrodeposited AC air cathode on the ORR activity, a series of power density measurements were performed in a MFC equipped with the same anode and different cathodes.

The results are shown in Fig. 6a, which obviously demonstrates that the electrodeposition of MnO_2 onto the AC air cathode

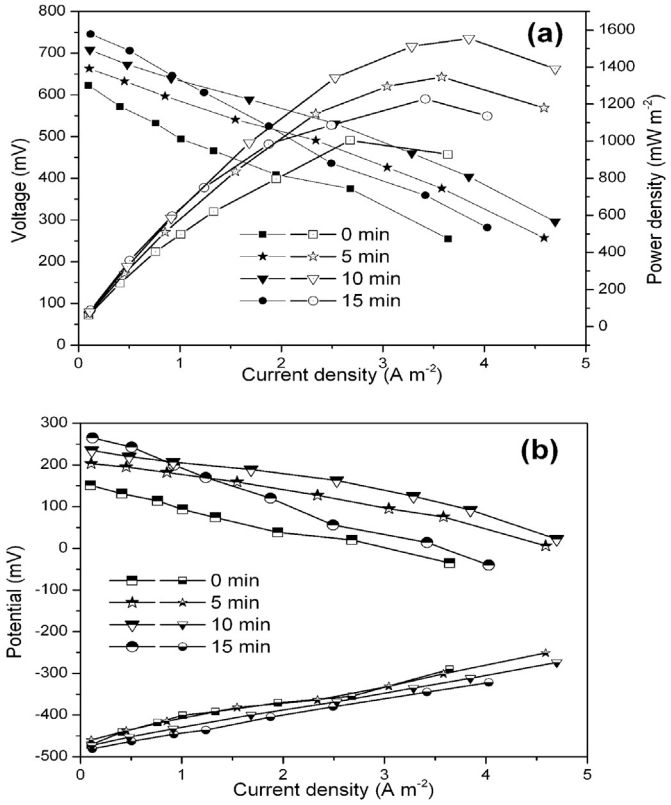

Fig. 6. Performance of MFCs equipped with a bare AC air cathode and electrodeposited-MnO_2 AC air cathodes with deposition times of 5, 10 and 15 min: (a) power density and cell voltage curves (power density: filled symbols; cell voltage: open symbols) and (b) cathode and anode polarisation curves (anode: the lower part of the symbol is filled; cathode: the upper part of the symbol is filled).

significantly affected the power performance. The MFC with the bare AC air cathode had a maximum power density of 1004 mW m^{-2}, which was similar to what had been previously reported [10,38]. When the deposition time increased from 0 to 10 min, the maximum power density was substantially enhanced. The AC air cathode with a MnO_2 deposition time of 5 min had a maximum power density of 1346 mW m^{-2}, which corresponds to a 1.34 times increased power output when compared to the unmodified AC air cathode. However, the AC air cathode with a MnO_2 deposition time of 10 min produced the maximum power density, 1554 mW m^{-2}, which was 1.5 times higher than that of the bare AC air cathode. However, as the deposition time increased further to 15 min, the maximum power density decreased to 1227 mW m^{-2}, which was lower than that of the AC cathodes with deposition times of 5 and 10 min.

The results showed that the maximum power output, which had also been affected by the specific surface area of the electrode, was not simply proportionate to the electrodeposited amount of MnO_2 [20]. The variation trend of maximum power density was consistent with the surface characteristic revealed by SEM (Fig. 2) and the BET surface area results, which had been previously reported by Chen et al. [20,39,40]. As the deposition time increased, the micropore surface area decreased sharply, but the maximum power output only decreased with deposition time of 15 min; this phenomenon showed that micropore may not have obvious boosting influence on the power output. The power output correlated with the mesoporous surface area, which indicated that the performance of the MnO_2-deposited AC air cathode was influenced by the mesoporous surface area. Higher mesopore surface area may bring about more amounts of active sites, which leads to much higher activity for ORR [40,41]. We inferred that, on the one hand, micropore can expand the surface area of electrode, but on the other hand the too narrow passages of the micropores (<2 nm) may hinder the mass transfer of oxygen and reduction product [35]. The specific mechanism of why mesopore benefits the power output will be explored further in our next study.

The maximum power density of the air cathode produced by the method described here was almost equal to that prepared with polydimethyl siloxane and Pt (1610 mW m^{-2}) [42], and higher than that with pure MnO_2 reported by Wen et al. [24]. The performance of the MFC reported here was obviously higher than the MnO_2 modified air cathode (88 ± 8 mW m^{-2}, MnO_2 as catalytic component and graphite as conductive material) reported by Zhang et al. [17]. The MnO_2 particles of the electrode were more than nano size, but the highest current density was slightly higher than the nanotubular MnO_2/graphene oxide composites; this may be because AC had bigger surface area than graphene oxide [16]. Furthermore, the preparation method used here is simpler, so this study could promote the practical utilisation of AC air cathodes. Undeniably, smaller size of the electrodeposited particles should also be explored to enhance its performance further.

The cathode and anode polarisation curves (Fig. 6b) demonstrated that the increase in cathode performance was responsible for enhancing the power output. It was obvious that there was an insignificant difference in the anode performances. In contrast, the variation in cathode polarisation curves was obvious and depended on the amount of MnO_2 deposited on the electrode. The open circuit potentials (OCP) of the MFCs varied in the same order as the LSV results, but the OCPs were slightly lower than the E_{onset} values displayed in Fig. 5, which may be due to the accumulation of microorganisms on the surface of the electrode, leading to a decrease in MFC performance [43] over time. The AC air cathode with a MnO_2 deposition time of 15 min had the highest E_{onset}, but the working potential of that cathode decreased faster with increasing current density than the other cathodes. This may be caused by the increased internal resistance of the electrode due to an overload of insulating MnO_2. In comparing the polarisation curves of the cathodes with deposition time, the cathode with a deposition time of 10 min exhibited the lowest slope, indicating the lowest overpotential for ORR [20].

The ORR mechanism on MnO_2 had been explained by the role of the Mn(IV)/Mn(III) redox couple. The MnO_2 was reduced to MnOOH [24], which was consequently reoxidized to Mn(IV) by oxygen. The mechanism was difficult to determine at neutral pH due to the low concentration of hydroxide ions. The 2-electron reduction pathway can yield peroxide ions as intermediates, which are corrosive [44] and can corrode the cathode. MnO_2 are able to prevent the formation of peroxide and promote their decomposition [45]. However, further researches about ORR mechanism of MnO_2 are necessary to be held to provide more insight on the reduction pathway in neutral conditions so that we can get better use of the MFC to harvest electricity power.

4. Conclusions

AC air cathodes containing electrodeposited γ-MnO_2 were produced using a simple potentiostatic method. The modified cathodes, especially the cathode with a deposition time of 10 min, exhibited higher catalytic activity for ORR than the bare AC air cathode. Carnation-like MnO_2 crystals bound to the surface of the AC air cathode were found to enhance the cathode performance. The BET analysis demonstrated that as deposition time increased, the micropore surface area decreased and the mesopore surface area first increased and then decreased. The highest maximum power density of 1554 mW m^{-2} was achieved with a MnO_2-deposited AC air cathode, which is comparable to that of a MFC with Pt as the cathode catalyst. Our results indicate that MnO_2 is a good alternative catalyst to Pt and that mesopores may play an important role in the cathode performance. The simple preparation method used for the AC air cathodes in this work increases the feasibility of the large-scale application of MFC technology.

Acknowledgements

This work is partially supported by the YIYUAN Environmental Research Fund (No. 2013-01) and the Marine Promotion Program from the Tianjin Oceanic Administration (No. KJXH2011-11).

References

[1] H. Liu, S. Cheng, B.E. Logan, Environ. Sci. Technol. 39 (2005) 658–662.
[2] R.A. Rozendal, H.V. Hamelers, K. Rabaey, J. Keller, C.J. Buisman, Trends Biotechnol. 26 (2008) 450–459.
[3] H. Liu, B.E. Logan, Environ. Sci. Technol. 38 (2004) 4040–4046.
[4] X. Xia, F. Zhang, X. Zhang, P. Liang, X. Huang, B.E. Logan, ACS Appl. Mater. Interfaces 5 (2013) 7862–7866.
[5] F. Zhang, S. Cheng, D. Pant, G.V. Bogaert, B.E. Logan, Electrochem. Commun. 11 (2009) 2177–2179.
[6] S. Cheng, H. Liu, B.E. Logan, Environ. Sci. Technol. 40 (2006) 364–369.
[7] I. Matanovic, P.R. Kent, F.H. Garzon, N.J. Henson, J. Phys. Chem. C 116 (2012) 16499–16510.
[8] P.D. Kiely, G. Rader, J.M. Regan, B.E. Logan, Bioresour. Technol. 102 (2011) 361–366.
[9] T. Saito, M.D. Merrill, V.J. Watson, B.E. Logan, M.A. Hickner, Electrochim. Acta 55 (2010) 3398–3403.
[10] H. Dong, H. Yu, H. Yu, N. Gao, X. Wang, J. Power Sources 232 (2013) 132–138.
[11] H. Dong, H. Yu, X. Wang, Environ. Sci. Technol. 46 (2012) 13009–13015.
[12] G. Chen, F. Zhang, B.E. Logan, M.A. Hickner, Electrochem. Commun. 34 (2013) 150–152.
[13] S. Cheng, J. Wu, Bioelectrochemistry 92 (2013) 22–26.
[14] X. Wang, N. Gao, Q. Zhou, H. Dong, H. Yu, Y. Feng, Bioresour. Technol. 144 (2013) 632–636.
[15] V.J. Watson, C.N. Delgado, B.E. Logan, J. Power Sources 242 (2013) 756–761.
[16] Z. Awan, K. Suk Nahm, J. Stanley Xavier, Biosens. Bioelectron. 53 (2014) 528–534.

[17] L. Zhang, C. Liu, L. Zhuang, W. Li, S. Zhou, J. Zhang, Biosens. Bioelectron. 24 (2009) 2825–2829.
[18] I. Roche, E. Chaînet, M. Chatenet, J. Vondrák, J. Phys. Chem. C 111 (2007) 1434–1443.
[19] X.-W. Liu, X.-F. Sun, Y.-X. Huang, G.-P. Sheng, K. Zhou, R.J. Zeng, F. Dong, S.-G. Wang, A.-W. Xu, Z.-H. Tong, Water Res. 44 (2010) 5298–5305.
[20] Y. Chen, Z. Lv, J. Xu, D. Peng, Y. Liu, J. Chen, X. Sun, C. Feng, C. Wei, J. Power Sources 201 (2012) 136–141.
[21] M. Lu, S. Kharkwal, H.Y. Ng, S.F.Y. Li, Biosens. Bioelectron. 26 (2011) 4728–4732.
[22] M. Lu, L. Guo, S. Kharkwal, H.n. Wu, H.Y. Ng, S.F. Yau Li, J. Power Sources 221 (2012) 381–386.
[23] S. Zhu, H. Zhou, M. Hibino, I. Honma, M. Ichihara, Adv. Funct. Mater. 15 (2005) 381–386.
[24] Q. Wen, S. Wang, J. Yan, L. Cong, Z. Pan, Y. Ren, Z. Fan, J. Power Sources 216 (2012) 187–191.
[25] H. Dong, H. Yu, X. Wang, Q. Zhou, J. Feng, Water Res. 46 (2012) 5777–5787.
[26] S. Chou, F. Cheng, J. Chen, J. Power Sources 162 (2006) 727–734.
[27] D.R. Lovley, E.J. Phillips, Appl. Environ. Microbiol. 54 (1988) 1472–1480.
[28] X. Wang, S. Cheng, Y. Feng, M.D. Merrill, T. Saito, B.E. Logan, Environ. Sci. Technol. 43 (2009) 6870–6874.
[29] J.M. Morris, S. Jin, J. Wang, C. Zhu, M.A. Urynowicz, Electrochem. Commun. 9 (2007) 1730–1734.
[30] L.-B. Kong, R.-J. Bai, J.-W. Lang, Y.-C. Luo, L. Kang, Russ. J. Electrochem. (2012) 1–8.
[31] S. Donne, A. Hollenkamp, B. Jones, J. Power Sources 195 (2010) 367–373.
[32] W.-H. Ryu, J.-H. Yoon, H.-S. Kwon, Mater. Lett. 79 (2012) 184–187.
[33] J. Yan, E. Khoo, A. Sumboja, P.S. Lee, Acs Nano 4 (2010) 4247–4255.
[34] H. Adelkhani, M. Ghaemi, J. Alloys Compd. 493 (2010) 175–178.
[35] V.J. Watson, C. Nieto Delgado, B.E. Logan, Environ. Sci. Technol. 47 (2013) 6704–6710.
[36] J. Chastain, R.C. King Jr., Perkin–Elmer Corp. 40 (1992) 221.
[37] B. Choi, S. Lee, C. Fushimi, A. Tsutsumi, Electrochim. Acta 56 (2011) 6696–6701.
[38] F. Zhang, D. Pant, B.E. Logan, Biosens. Bioelectron. 30 (2011) 49–55.
[39] M.A. Hasan, M.I. Zaki, L. Pasupulety, K. Kumari, Appl. Catal. A Gen. 181 (1999) 171–179.
[40] W. Zhang, H. Wang, Z. Yang, F. Wang, Colloids Surf. A Physicochem. Eng. Aspects 304 (2007) 60–66.
[41] Y.-s. Ding, X.-f. Shen, S. Sithambaram, S. Gomez, R. Kumar, V.M.B. Crisostomo, S.L. Suib, M. Aindow, Chem. Mater. 17 (2005) 5382–5389.
[42] F. Zhang, M.D. Merrill, J.C. Tokash, T. Saito, S. Cheng, M.A. Hickner, B.E. Logan, J. Power Sources 196 (2011) 1097–1102.
[43] B. Wei, J.C. Tokash, G. Chen, M.A. Hickner, B.E. Logan, RSC Adv. 2 (2012) 12751–12758.
[44] M. Chatenet, L. Géniès-Bultel, M. Aurousseau, R. Durand, F. Andolfatto, J. Appl. Electrochem. 32 (2002) 1131–1140.
[45] I. Roche, K. Katuri, K. Scott, J. Appl. Electrochem. 40 (2010) 13–21.